



An incremental iterative solution procedure without predictor step

Mohammad Rezaiee-Pajand  and Hossein Afsharimoghadam

Department of Civil Engineering, Ferdowsi University of Mashhad, Mashhad, Iran

ABSTRACT

Geometric non-linear analyses are performed utilising two main control factors, including load and displacement parameters. In this paper, a new incremental-iterative scheme without predictor step is suggested. Using the obtained constraint equation, the load factor increment is calculated. It is assumed that the path corresponding to the iterative analysis is a parabolic curve. Two different mathematical procedures are developed in order to form this new constraint equation. In the first formulation, two reasonable assumptions are considered for the parabolic path. The length of iterative steps' curve is minimised in the second scheme. To corroborate the efficiency and capability of the proposed technique, several structures with complex non-linear behaviour are solved.

ARTICLE HISTORY

Received 16 June 2017
Accepted 17 March 2018

KEYWORDS

Structural equilibrium path;
geometrically non-linear
behaviour; minimisation;
parabolic iterative steps;
space frame

1. Introduction

Structural analysis can be performed linearly or non-linearly. In the linear analysis, a simple behaviour is considered for structures. Note that this behaviour is unrealistic when large loads are applied to the structures or thin members are used. To achieve accurate responses, non-linear analyses are required for this condition. The response of structures might include material and/or geometric nonlinearities. In the geometric non-linear analysis, the initial shape of the structure is changed because of large deformations. Thus far, various strategies have been proposed to conduct the geometric non-linear analysis of the structures.

One of the old and elementary analysis methods is named pure incremental strategy. This algorithm performs weakly in the problems with large displacements and rotations (Chajes & Churchill, 1987). In addition, more efficient techniques in the structural non-linear analysis are the incremental-iterative tactics, such as well-known Newton-Raphson scheme. In each step of Newton-Raphson method, the load level is constant. In this procedure, the stiffness matrix is required to be

updated successively. As a result, this approach is computationally expensive and slow to perform for the structures with a large number of degrees of freedom. To remove these deficiencies, the modified Newton-Raphson algorithm was suggested. In this technique, the stiffness matrix is only calculated at the beginning of each step, and this matrix is used for the other iterations throughout the increment (Crisfield, 1979). It should be noted, this way is not able to trace the load limit points, appropriately. Considering the weakness of this strategy, the displacement control scheme was proposed. Accordingly, a displacement component is assumed to be constant in the iterations of each increment.

Note that the aforementioned tactic fails in presenting the snap-back regions of the structural equilibrium path (Zienkiewicz, 1971). For solving this issue, Wempner and Riks suggested the arc length algorithms. The related constraint equations define the distance between the last equilibrium point and iterative analyses path (Riks, 1972; Wempner, 1971). This route is named arc length, and should be defined as a constant value in the first iteration. Moreover, several researchers have suggested some orthogonal methods. For instance, the normal plane procedure and updated normal plane approach are the oldest and most famous ones (Ramm, 1981; Riks, 1979). In the same area of study, Fried developed the orthogonal vector method (Fried, 1984). Crisfield ignored the load factor in the constraint equation of the cylindrical arc length strategy and proposed the updated-Wempner-Riks approach (Crisfield, 1981). In another study, Simons et al. organised the normal unbalanced displacement strategy utilising all the entries of the displacement vector in the solution procedure (Simons, Bergan, & Nygard, 1984). Moreover, Rezaiee-Pajand and Tatar found other constraint equations by applying the orthogonal condition (Rezaiee-Pajand & Tatar, 2006).

In 1981 and 1985, the work control scheme was presented in which the work increment was supposed to be constant at each step (Powell & Simons, 1981; Yang & McGuire, 1985). In another research, the normal flow approach was established based on the iterative analysis, which is performed on the perpendicular lines to Davidenko's flow. Changing the perturbation coefficient could generate Davidenko's flow curves (Allgower & Georg, 1979). The modified version of this method was presented by Saffari et al. (Saffari, Fadaee, & Tabatabaei, 2008). Recently, the angle between the predictor and corrector path was assessed. Rezaiee-Pajand and Afsharimoghadam took advantage of two-variable objective functions and obtained two new constraint equations for geometric nonlinear analysis (Rezaiee-Pajand & Afsharimoghadam, 2017).

As yet, various methods have been proposed for reaching the responses of the structural equilibrium path, one of which is based on mixing the orthogonal tactics with Quasi-Newton procedures (Krenk & Hededal, 1995). In another publication, Rezaiee-Pajand and Boroshaki recommended the variant arc length method for assessing the nonlinear behaviour of the structures (Rezaiee-Pajand & Boroshaki, 1999). Kim and Kim employed neural networks and Newton-Raphson algorithms in the predictor and corrector steps, respectively (Kim & Kim, 2001). In 2004, the

non-linear analyses of the trusses were performed by minimising the total energy of the structure (Toklu, 2004). Similarly, using analytical formulation, Ligaro and Valvo minimised the structural total energy to evaluate the nonlinear behaviour of the regular pyramid truss (Ligaro & Valvo, 2006).

Several researchers have attempted to minimise a few of the residual parameters so as to guarantee the process convergence in the analysis steps. In the other words, an attempt was made to close the estimated responses to the true structural equilibrium path. Herein, Bergan proposed a new relation by minimising the reduced residual load (Bergan, 1980). In 1988, Chan suggested a method in which the residual displacements were minimised. In this procedure, the displacement criterion was used to finish the iterations of each increment. It is worth emphasising that this method traces the shortest path to achieve the solution convergence (Chan, 1988). To pass the load and displacement limit points, Yang and Shieh proposed the generalised displacement control strategy (Yang & Shieh, 1990). Cardoso and Fonseca reflected that the generalised displacement control technique is the same as the normal cylindrical arc length technique (Cardoso & Fonseca, 2007). In another study, Rezaiee-Pajand and Tatar suggested the residual length minimisation algorithm (Rezaiee-Pajand & Tatar, 2009). Similarly, by utilising the geometric approach, the area and perimeter of a residual rectangular were minimised in the iterative steps (Rezaiee-Pajand, Tatar, & Moghaddasie, 2009).

It is significant to mention that the arc length formulation can be applied in both load and displacement spaces. However, this way brings about numerical difficulties. In order to ease this process, Krishnamoorthy et al. proposed a three-parameter arc length method. It is important to note that, the constraint equations are dimensionless in this scheme (Krishnamoorthy, Ramesh, & Dinesh, 1996). In an extensive study, the capabilities of the different geometric non-linear analysis approaches were compared (Rezaiee-Pajand, Ghalishooyan, & Salehi-Ahmadabad, 2013).

As a different way, the dynamic relaxation (DR) algorithm was employed for the post-buckling analysis of the trusses (Papadrakakis, 1983). In fact, the dynamic relaxation method is an explicit approach for solving the simultaneous systems of equations. In this kind of non-linear solver, the fictitious mass and damping are added to the static governing equations, and an artificial dynamic system is built for the structural behaviour. Several ways of formulating these strategies are available in the related literature (Rezaiee-Pajand & Alamatian, 2008, 2010, 2011; Rezaiee-Pajand, Kadkhodayan, Alamatian, & Zhang, 2011; Rezaiee-Pajand & Sarafrazi, 2010, 2011; Rezaiee-Pajand & Taghavian-Hakkak, 2006). In the recent years, Rezaiee-pajand et al. have performed many nonlinear structural analyses by these procedures (Rezaiee-Pajand, Kadkhodayan, & Alamatian, 2012; Rezaiee-Pajand, Sarafrazi, & Rezaiee, 2012; Rezaiee-Pajand & Rezaee, 2014; Rezaiee-Pajand & Estiri, 2016a, 2016b, 2016c, 2016d).

In what follows, the studies conducted on the stiffness of the frame structures are reviewed briefly. In 1965, the first geometric non-linear stiffness matrix of the

frame structures was formulated (Saafan, 1965). Later, Connor et al. used a simple stiffness matrix in specific conditions (Connor, Logcher, & Chan, 1968). Tezcan and Mahapatra applied the updated Lagrangian method to formulate a simple stiffness matrix for three-dimensional frame members with small deformations. This stiffness matrix is asymmetric, and it is unsuitable for the non-prismatic members (Tezcan & Mahapatra, 1969). In another study, Oran found a symmetric stiffness matrix for the plane and space frame members with small deformations and large rotations (Oran, 1973a, 1973b). In 1973, the elastic frame structures and beams were analysed via simple equalities (Yang, 1973). Wen and Rahimzadeh considered small nodal rotations and large member deformations for analysing the frame structures. They developed a tangential stiffness matrix which is successful in the analysis of the structures with small displacements, although it was required to be modified for those with large displacements (Wen & Rahimzadeh, 1983). In another research, Meek et al. used the third-order deformations and large rotations for the analysis of the space frames. They took advantage of the suitable shape functions to account for large deformations in the analysis (Meek & Loganathan, 1989; Meek & Tan, 1984). Furthermore, applying the virtual work principle and non-linear strains contribute towards obtaining a new stiffness matrix, including two parts, for the three-dimensional beams with non-uniform torsion (Yang & McGuire, 1986).

Spillers utilised Taylor's expansion series and equilibrium equation to develop the asymmetric stiffness matrix for the space frames with large rotations and small rotational strains (Spillers, 1990). In 1992, the multi-storey frames were assessed under the distributed loads. In this process, the curvature and warping effects of the members were inserted into the chordal stiffness matrix (Singh & Singh, 1992). Considering the small strains and medium to large rotations for the members, Torkamani et al. performed the second-order geometric non-linear analysis on the 2D frames (Torkamani, Sonmez, & Cao, 1997). Furthermore, Chang proposed the higher order stiffness matrix of the 3D frames by employing the rigid body principle. This matrix included the elastic, geometric and higher order parts (Chang, 2004). In another work, the geometric stiffness matrices of the curved beams were used in their buckling analysis. Note that the stiffness matrices of these beams were achieved by changing the Cartesian coordinates of the straight beams into the cylindrical coordinates (Yang, Lin, & Wang, 2007).

According to the literature review, it can be concluded that in the previous approaches, the predictor and corrector steps were employed for achieving the true behaviour of the structures. In this paper, a parabolic path is utilised for the iterative analyses. As a usual way of the incremental solutions, the tangential stiffness matrix is employed. In contrast to the previous strategies, the suggested method does not require the predictor step. Although, two completely different mathematical approaches are utilised throughout this study, only one constraint equation is derived. This is an indication that the presented method is mathematically valid even before performing numerical tests. In the first formulation,

a new constraint equation is obtained, based on two appropriate assumptions for the parabolic path. In the other scheme, in which Bernoulli's equivalence relation is used, the same new equality is acquired through minimising the iterative path length. To verify the outcomes of this study, some structural geometric nonlinear analyses are performed. As it will be shown, extended numerical experiences clearly demonstrate that authors' method can automatically implement structural analysis without the intervention of the analyst.

2. General structural non-linear analysis

The equilibrium path of a structure depends on the applied loads and structural geometry. To satisfy the equilibrium condition, common governing equations are written in the below form:

$$R(u, \lambda) = \lambda P - F(u) \quad (1)$$

In this relation, the displacement vector, load factor, residual load vector, external force vector, and internal force vector are denoted by u , λ , R , P and F , respectively. The residual force vector is a function of the displacements and load factor. It is worth emphasising that the load factor is an important parameter in the non-linear analysis process. If the displacement vector includes m entries, the number of the structural unknowns will be $m + 1$. Inserting the load factor into the formulations, produces an extra unknown. Consequently, a different equation is required in addition to Equation (1). According to Figure 1, in the n -th increment, the part of the equilibrium path which begins at the $(n - 1)$ -th point and finishes at the n -th point is obtained. In the first iteration, the incremental load factor can be computed, based on several assumptions. Hence, related displacements can be computed using the next relation:

$$\Delta u_1^n = (K^{n-1})^{-1} \times \Delta \lambda_1^n P \quad (2)$$

In the current equality, the tangential stiffness matrix at the $(n - 1)$ -th equilibrium point is denoted by K^{n-1} . The displacement increment and load factor of the initial iteration are denoted by Δu_1^n and $\Delta \lambda_1^n$, correspondingly. To reach the n -th point, the sequential iterations are needed. For each iteration, the load factor is computed by means of the constraint equation. Utilising a linear combination of the increment of the related displacements to the residual load and external force in each iteration, results in the displacement increment as follows (Batoz & Dhatt, 1979):

$$\delta u_i^n = \delta u_i''^n + \delta \lambda_i^n \delta u_i'^n \quad (3)$$

Where, superscript n and subscript i denote the increment and iteration number, respectively. Furthermore, $\delta u_i'^n$ and $\delta u_i''^n$ are the displacement increments induced

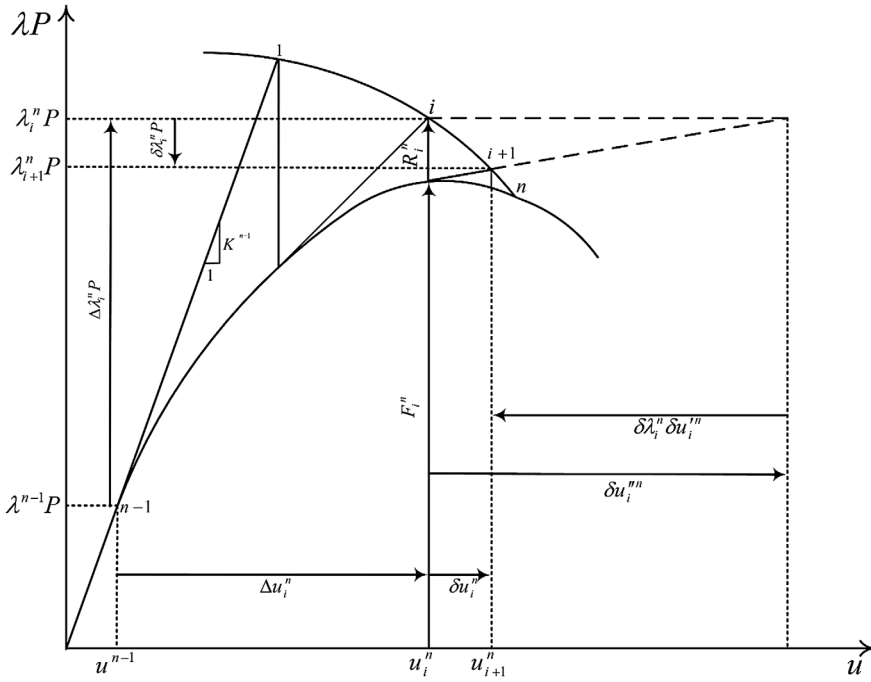


Figure 1. The common incremental-iterative methods, including predictor and corrector steps.

by the external force and residual load, correspondingly. These displacements are given by the subsequent equalities:

$$\delta u_i^{n,n} = (K_i^n)^{-1} \times P \quad (4)$$

$$\delta u_i^{n,n} = (K_i^n)^{-1} \times R_i^n \quad (5)$$

It is noteworthy that the internal and external forces are known at the beginning of each iteration. Therefore, the dependent displacement increments are available. According to Equation (3), only $\delta \lambda_i^n$ is required for computing the displacement increment in the corrector step. Finally, the incremental load factor and the displacement increment of the next step can be obtained by adding $\delta \lambda_i^n$ and δu_i^n to their previous increments, respectively. Thus, they have the following forms:

$$\Delta \lambda_{i+1}^n = \Delta \lambda_i^n + \delta \lambda_i^n \quad (6)$$

$$\Delta u_{i+1}^n = \Delta u_i^n + \delta u_i^n \quad (7)$$

It should be added that the load factor increment is computed in each iteration using the constraint equation. In this work, the path of the iterative analyses is assumed to be a parabolic curve. To solve the equilibrium equation, the tangential stiffness matrix is employed in the formulation. Considering that authors'

approach does not need the predictor step, it is more efficient compared to the tactics proposed by the former studies. In this paper, the load factor increment is calculated using an iterative process. It will be extensively demonstrated that the suggested technique can automatically perform the structural geometric nonlinear analysis.

In order to simplify the presented formulation, a single degree of freedom structure is considered while deriving the constraint equation. Thus, all vectors and matrices used in the process of the proposed formulations become scalars, and generating algebraic expressions. Finally, the same constraint equality that has been obtained by two different approaches is generalised for the analysis of multi-degree of freedom structures and converted to vector space. For these cases, matrix notation applies.

2.1. First suggested formulation

By assuming that the iterative paths have the parabolic shape in each increment, the succeeding constraint equation can be achieved:

$$\lambda_{i+1}^n P = a \times (u_{i+1}^n)^2 + b \times u_{i+1}^n + c \quad (8)$$

In this equation, a , b and c are constant values due to supposing that there is one entry in the load and displacement vector. Based on Figure 2, by transferring the coordinate system to the $(n - 1)$ -th equilibrium point, the constraint equation is derived in the new coordinate system. Additionally, by inserting the coordinates of the $(n - 1)$ -th point into the new coordinate system; the constant value c will be equal to zero in the relation (8). For the mentioned condition, the following relationships are held:

$$\Lambda_{i+1}^n P = a \times (U_{i+1}^n)^2 + b \times U_{i+1}^n \quad (9)$$

$$U_{i+1}^n = \Delta u_i^n + \delta u_i^n \quad (10)$$

$$\Lambda_{i+1}^n P = \Delta \lambda_i^n P + \delta \lambda_i^n P \quad (11)$$

In these equalities, U and Λ denote the displacement and load factor in the new coordinate system, respectively. After finding coefficients a and b via the relation (9), the constraint equation can be obtained. To achieve this goal, two reasonable assumptions should be made. Firstly, it is presumed that the tangent of the equilibrium path and iterative analysis one are equal at the beginning of each increment. This issue can be expressed mathematically as below:

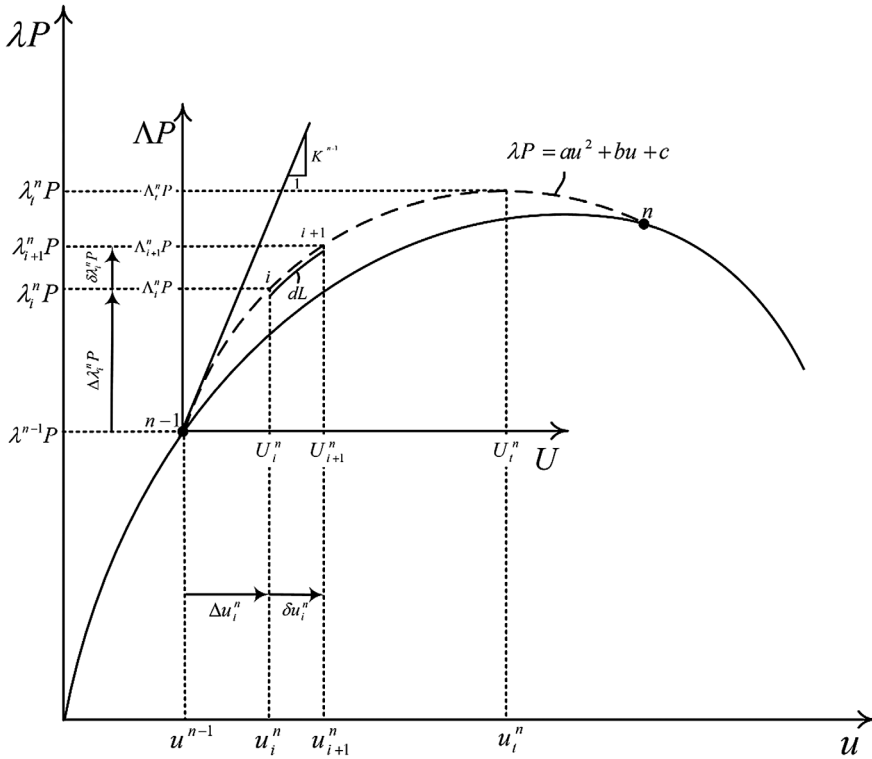


Figure 2. The iterative path of the suggested technique and its dependent variables.

$$\left. \frac{\partial \Lambda P}{\partial U} \right|_{U=0} = K^{n-1} \quad (12)$$

From the geometrical viewpoint, this analogy is shown in Figure 2. Using Equation (12), parameter b in Equation (9) can be computed as the coming form:

$$b = K^{n-1} \quad (13)$$

Herein, the second assumption is introduced. According to Figure 2, if the parabolic path includes an extreme point, the tangent to this curve is horizontal at the point $(U_t^n, \Lambda_t^n P)$. Consequently, calculating the derivative of the relation (9), substituting U_{i+1}^n with U_t^n , and setting the obtained result to zero, lead to the succeeding formula:

$$U_t^n = -\frac{b}{2a} \quad (14)$$

Then, inserting the extreme point coordinates into Equation (9), and utilising the current equality result in the next relation:

$$a = -\frac{b^2}{4\Lambda_i^n P} \quad (15)$$

By substituting the parameter obtained from Equation (13) in the above-cited relation, Equation (15) can be rewritten as below:

$$a = -\frac{(K^{n-1})^2}{4\Lambda_i^n P} \quad (16)$$

Hence, inserting parameters a and b into Equation (9) yields the coming result:

$$\Lambda_{i+1}^n P = -\frac{(K^{n-1})^2 \times (U_{i+1}^n)^2}{4\Lambda_i^n P} + K^{n-1} U_{i+1}^n \quad (17)$$

It should be reminded that parameters a and b are achieved by the relations (16) and (13), respectively. Utilising Equations (3), (10) and (11), and also inserting them into the last equality, the constraint equation can be simplified as the next form:

$$A(\delta\lambda_i^n)^2 + B(\delta\lambda_i^n) + C = 0 \quad (18)$$

$$\begin{aligned} A &= (K^{n-1})^2 (\delta u_i'^n)^2 \\ B &= 2(K^{n-1})^2 \Delta u_i^n \delta u_i'^n + 2(K^{n-1})^2 \delta u_i'^n \delta u_i''^n - 4K^{n-1} \Delta \lambda_i^n P \delta u_i'^n + 4\Delta \lambda_i^n P^2 \\ C &= (K^{n-1})^2 (\Delta u_i^n)^2 + 2(K^{n-1})^2 \Delta u_i^n \delta u_i''^n + (K^{n-1})^2 (\delta u_i''^n)^2 + 4\Delta \lambda_i^n \Delta \lambda_i^n P^2 \\ &\quad - 4K^{n-1} \Delta \lambda_i^n P \Delta u_i^n - 4K^{n-1} \Delta \lambda_i^n P \delta u_i''^n \end{aligned} \quad (19)$$

By ignoring the force component, P , in the coefficients of Equation (18), a double root can be derived for this quadratic algebraic equation. Subsequently, the only real root is presented in vector space as below:

$$\delta\lambda_i^n = -\frac{\Delta u_i^{nT} \delta u_i'^n + \delta u_i'^{nT} \delta u_i''^n}{\delta u_i'^{nT} \delta u_i''^n} \quad (20)$$

The current constraint equation can be applied for the iterative steps of the structural geometric nonlinear analysis. Since the frame's stiffness was reviewed in the present paper, several space frames are solved in this study.

2.2. Second suggested formulation

To find the constraint equation, another technique is utilised. In this method, the length of the parabolic path, shown in Figure 2, is minimised. As it was indicated

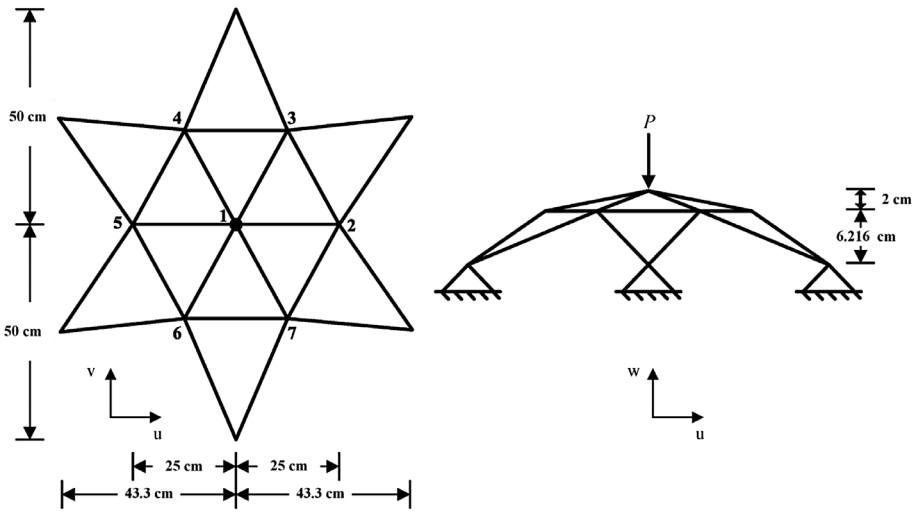


Figure 3. The plan and view of the star-shaped frame under a concentrated load.

before, a single degree of freedom structure is considered to simplify the formulation's process. Lastly, the obtained scheme is generalised for the wide-ranging structures.

The coming integration is used for calculating the arc length of the iterative path:

$$L = \int_{U_i^n}^{U_{i+1}^n} \sqrt{1 + \left(\frac{\partial \Delta P}{\partial U}\right)^2} dU \quad (21)$$

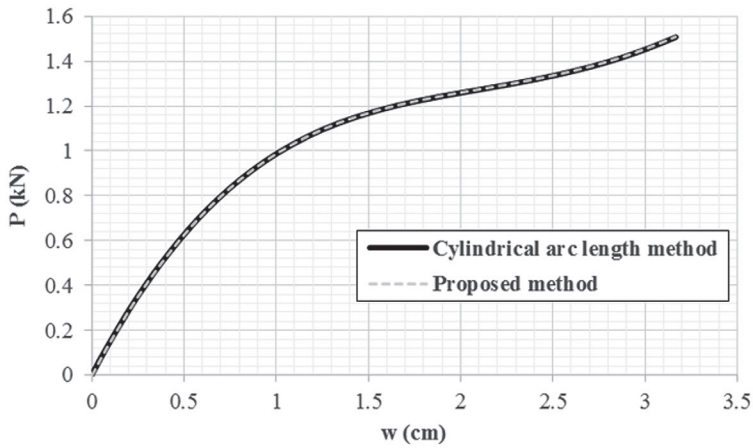
After computing the derivative of the parabolic relation (9), with respect to the displacement component, the above-mentioned integration can be rewritten as the following form:

$$L = \int_{U_i^n}^{U_{i+1}^n} \sqrt{1 + (2aU + b)^2} dU \quad (22)$$

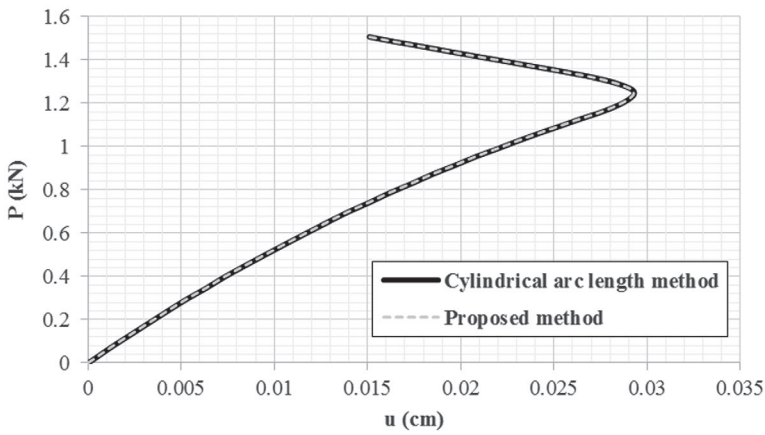
Since it is hard to solve analytically the last algebraic integration, an approximate approach can ease the calculation. In fact, in order to find the square root of the quadratic equation in the current integral, Bernoulli's equivalence relation is employed. Accordingly, Equation (22) converts to the following relation:

$$L \approx \int_{U_i^n}^{U_{i+1}^n} \left[1 + \frac{(2aU + b)^2}{2} \right] dU \quad (23)$$

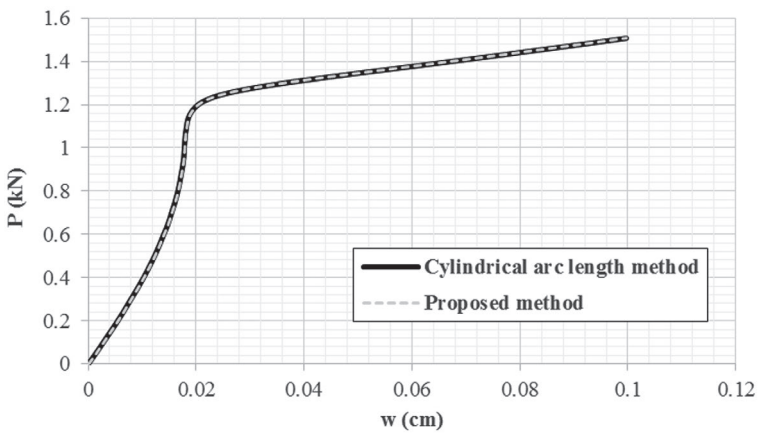
Similar to the previous suggested tactic, it is presumed that the tangents of the equilibrium path and parabolic curve are equal to the tangent stiffness matrix at



(a)



(b)



(c)

Figure 4. The equilibrium paths of the star-shaped frame with high rigidity. (a) The behavioural curve of node 1 in the z direction; (b) The behavioural curve of node 2 in the x direction; (c) The behavioural curve of node 2 in the z direction.

the beginning of each increment. Therefore, by replacing Equation (13) in the relation (23) and employing the equality (10) for the integral bounds, the subsequent result is obtained:

$$L \approx \left[\frac{2}{3} \times (\delta u_i^n)^3 + 2\Delta u_i^n (\delta u_i^n)^2 + 2\delta u_i^n (\Delta u_i^n)^2 \right] a^2 + \left[K^{n-1} (\delta u_i^n)^2 + 2K^{n-1} \Delta u_i^n \delta u_i^n \right] a + \delta u_i^n + \frac{1}{2} \times \delta u_i^n (K^{n-1})^2 \quad (24)$$

To find the optimum value of parameter a , the current arc length is minimised. By calculating the derivative of Equation (24) with respect to parameter a and setting it to zero, this parameter can be obtained as follows:

$$a = -\frac{3K^{n-1}(\delta u_i^n + 2\Delta u_i^n)}{4[(\delta u_i^n)^2 + 3\Delta u_i^n \delta u_i^n + 3(\Delta u_i^n)^2]} \quad (25)$$

Then, by inserting the relations (25) and (13) into Equation (9), and also employing the equalities (3), (10) and (11), the succeeding third-order formula is concluded with respect to the load factor increment:

$$A'(\delta \lambda_i^n)^3 + B'(\delta \lambda_i^n)^2 + C'(\delta \lambda_i^n) + D' = 0 \quad (26)$$

$$\begin{aligned} A' &= -K^{n-1}(\delta u_i^n)^3 + 4P(\delta u_i^n)^2 \\ B' &= -4K^{n-1}\Delta u_i^n(\delta u_i^n)^2 - 3K^{n-1}\delta u_i^n(\delta u_i^n)^2 + 4\Delta \lambda_i^n P(\delta u_i^n)^2 \\ &\quad + 12P\Delta u_i^n \delta u_i^n + 8P\delta u_i^n \delta u_i^n \\ C' &= -9K^{n-1}(\Delta u_i^n)^2 \delta u_i^n - 8K^{n-1}\Delta u_i^n \delta u_i^n \delta u_i^n - 3K^{n-1}\delta u_i^n (\delta u_i^n)^2 \\ &\quad + 12\Delta \lambda_i^n P \Delta u_i^n \delta u_i^n + 8\Delta \lambda_i^n P \delta u_i^n \delta u_i^n + 12P(\Delta u_i^n)^2 + 12P\Delta u_i^n \delta u_i^n + 4P(\delta u_i^n)^2 \\ D' &= -6K^{n-1}(\Delta u_i^n)^3 - 9K^{n-1}(\Delta u_i^n)^2 \delta u_i^n - 4K^{n-1}\Delta u_i^n (\delta u_i^n)^2 \\ &\quad - K^{n-1}(\delta u_i^n)^3 + 12\Delta \lambda_i^n P(\Delta u_i^n)^2 + 12\Delta \lambda_i^n P \Delta u_i^n \delta u_i^n + 4\Delta \lambda_i^n P(\delta u_i^n)^2 \end{aligned} \quad (27)$$

It should be mentioned that this third-order algebraic equation only has one real root. By ignoring the force component, P , in coefficients A' , B' , C' and D' , the real root leads to the same former constraint equation, which was given by the relation (20). Accordingly, the validity of the assumptions and formulations is proved. Indeed, reaching both presented procedures to an analogous constraint equation can verify the correctness of each other. As demonstrated so far, this is in spite of using the completely different mathematical approaches. Recall that; in order to analyse the multi-degree of freedom structures, the equality (20) is generalised to the vector space.

Table 1. The number of the increments and iterations of the star-shaped frame with high rigidity.

Technique	Number of increments	Number of iterations
Proposed method	172	1376
Cylindrical arc length method	242	798

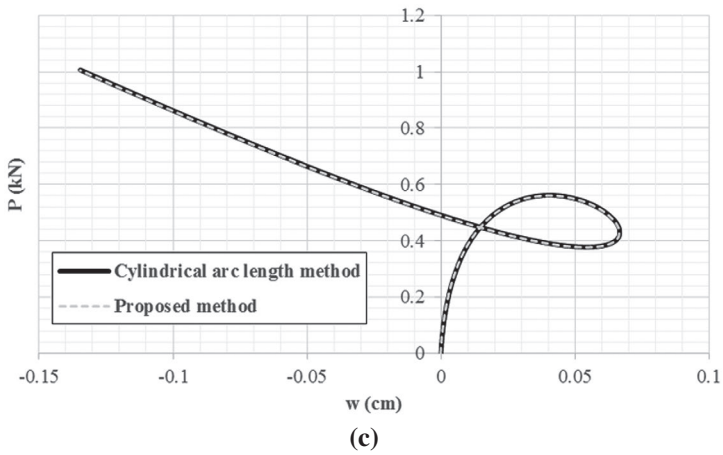
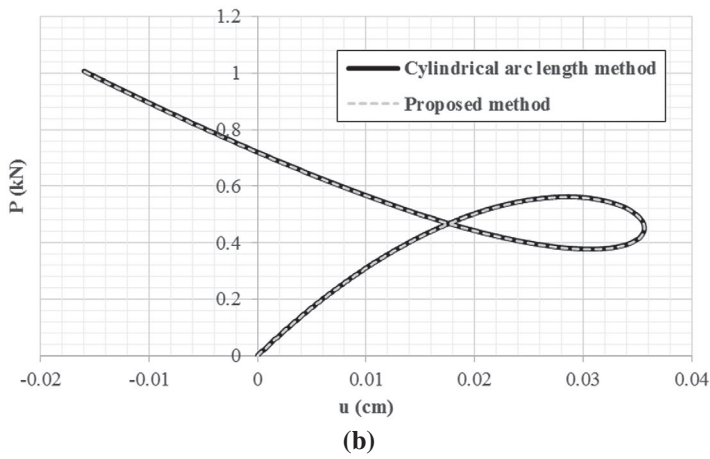
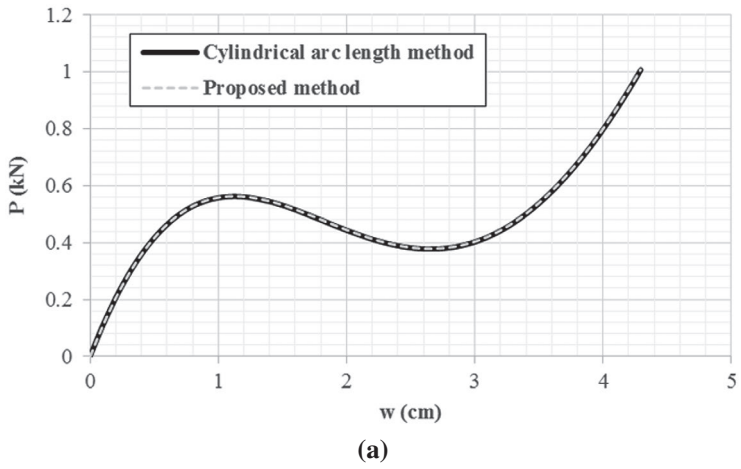


Figure 5. The load-deflection diagrams of the star-shaped frame with low rigidity under a concentrated load. (a) The behavioural curve of node 1 in the z direction; (b) The behavioural curve of node 2 in the x direction; (c) The behavioural curve of node 2 in the z direction.

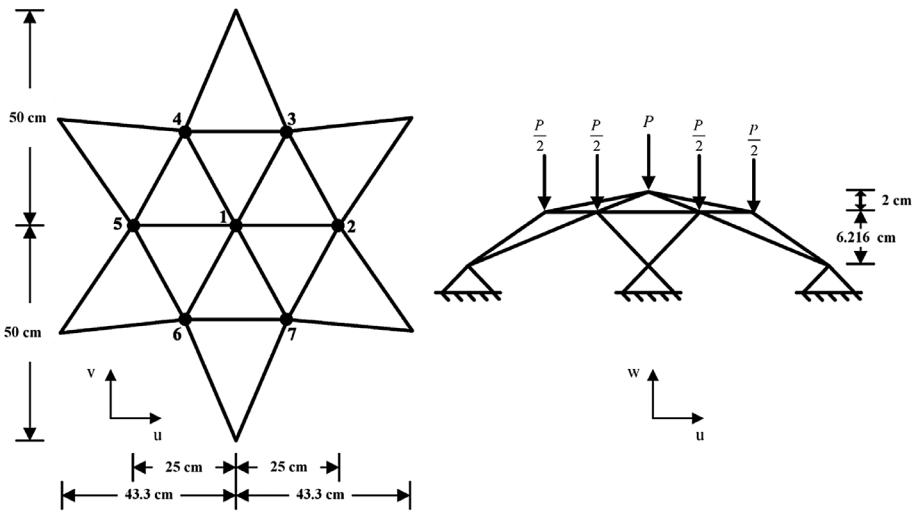


Figure 6. The plan and view of the star-shaped frame with low rigidity under symmetric loading pattern.

Table 2. The number of the increments and iterations of the star-shaped frame with low rigidity under a concentrated load.

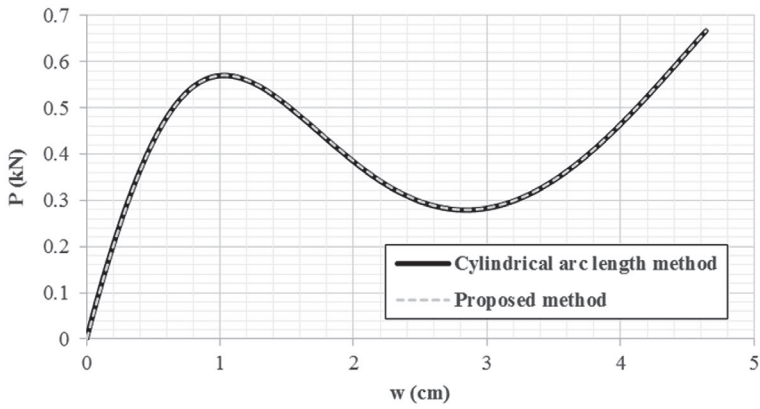
Technique	Number of increments	Number of iterations
Proposed method	490	3087
Cylindrical arc length method	686	1920

3. Numerical evaluations

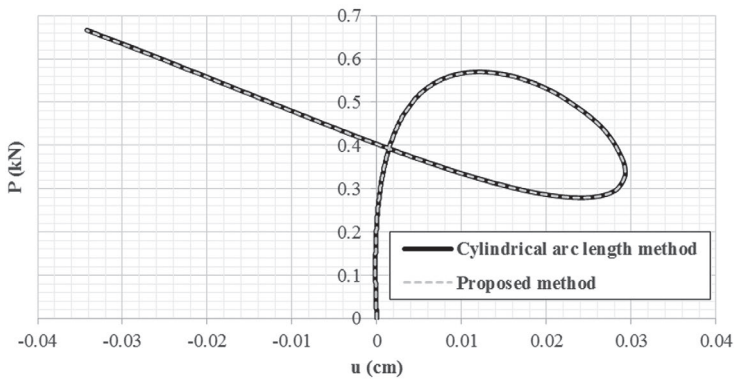
The geometric non-linear behaviours of the various space frames are studied via authors' computer programme. In this package, the proposed constraint relation (20) is employed. In addition to the benchmark problems, several novel 3D frames are analysed by the new formula. Besides, all of these structures are analysed utilising the common cylindrical arc length scheme. In this way, the capability of the new strategy to trace the complex static curves is evaluated. In all analysis processes, the allowable error is considered as 10^{-4} .

3.1. Star-shaped frame with high rigidity

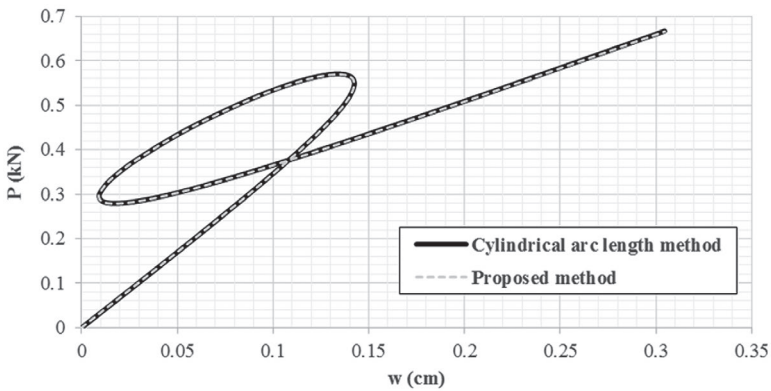
This benchmark structure has 13 nodes and 24 members. Figure 3 illustrates the star-shaped frame. A concentrated load, P , is applied to the top node. All exterior nodes of this structure are simply supported. The elasticity and shear modulus of the members are $E = 303 \text{ kN/cm}^2$ and $G = 109.6 \text{ kN/cm}^2$, respectively. Furthermore, the cross-sectional area, the bending and torsional moments of inertia are $A = 3.17 \text{ cm}^2$, $I_y = I_z = .837 \text{ cm}^4$, and $J = 1.411 \text{ cm}^4$, correspondingly. This benchmark structure was nonlinearly analysed using an incremental-iterative scheme in Meek and Tan's research (Meek & Tan, 1984). In another study, a three-dimensional beam member



(a)



(b)



(c)

Figure 7. The equilibrium curves of the star-shaped frame with low rigidity under symmetric loading pattern. (a) The load-displacement diagram of node 1 in the z direction; (b) The load-displacement diagram of node 2 in the x direction; (c) The load-displacement diagram of node 2 in the z direction.

with large rotations was proposed (Hsiao, Horng, & Chen, 1987). This member is used during the analysis of the star-shaped space frame.

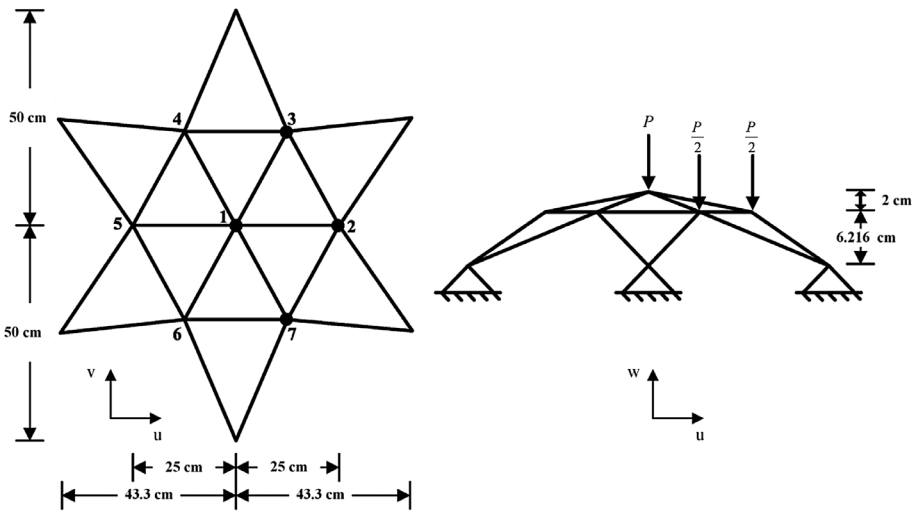


Figure 8. The plan and view of the star-shaped frame with low rigidity under asymmetric loading pattern.

Firstly, the equilibrium path of node 1 in the applied load's direction is achieved. According to Figure 4(a), the suggested approach can represent the equilibrium curve of this benchmark structure. The same solution is obtained by the cylindrical arc length approach. Moreover, the static curves of node 2 in the x and z directions are achieved successfully, and presented in Figure 4(b) and (c), correspondingly. Due to the high rigidity of this structure, no limit point is observed in Figure 4(a) and (c). However, Figure 4(b) includes a sharp snap-back region. According to the findings, authors' formula was capable of accurately tracing all mentioned equilibrium paths.

In Table 1, the number of the required increments and iterations, when using the relation (20) and cylindrical arc length tactic are listed. Accordingly, the new strategy brings about the responses with fewer increments and more iterations in comparison to the cylindrical arc length scheme.

3.2. Star-shaped frame with low rigidity under a concentrated load

Figure 3 shows this 3D frame structure. A concentrated load, P , is applied to the peak node of the frame. The elasticity and shear modulus of the members are $E = 303 \text{ kN/cm}^2$ and $G = 109.6 \text{ kN/cm}^2$, respectively. The cross-sectional area, the moment of inertia around the y and z axes are $A = 3.17 \text{ cm}^2$, $I_y = .295 \text{ cm}^4$, and $I_z = 2.377 \text{ cm}^4$, correspondingly. Moreover, the torsional moment of inertia of the structural members is equal to $J = .918 \text{ cm}^4$. Note that; the flexural and torsional rigidity of the members are less than those of the previous sample. Meek and Tan solved this benchmark frame (Meek & Tan, 1984). Besides, the dynamic post-buckling analysis of the star-shaped structure with large deformations was performed (Meek & Xue, 1998). In another research, the 3D benchmark frame,

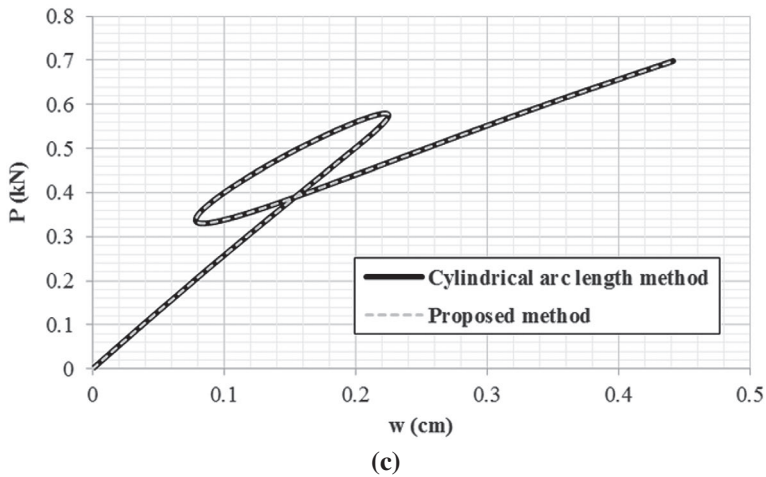
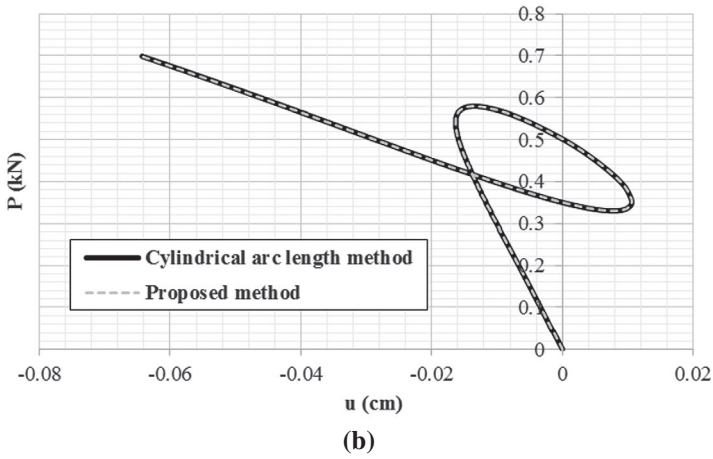
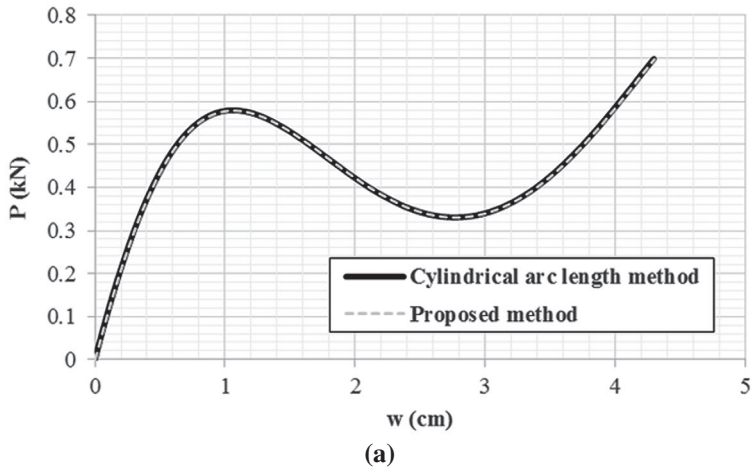
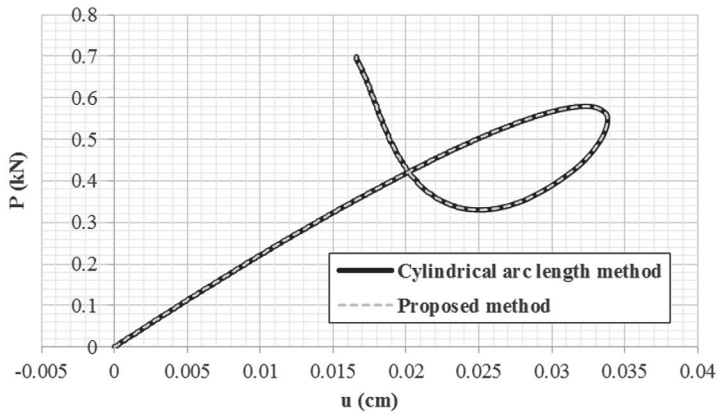
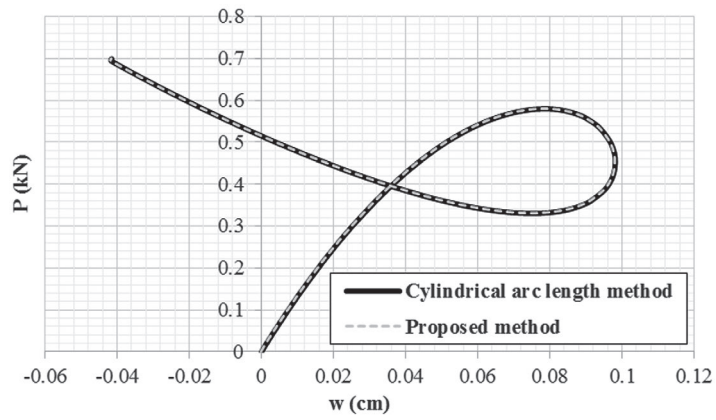


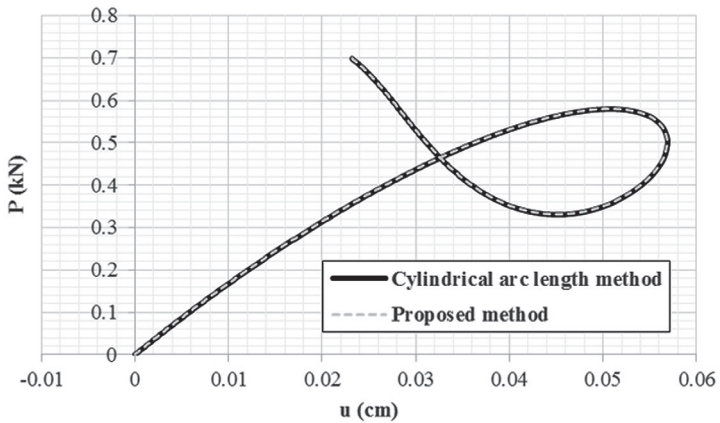
Figure 9. The load-displacement diagrams of the star-shaped frame with low rigidity under asymmetric loading pattern. (a) The equilibrium path of node 1 in the z direction; (b) The equilibrium path of node 2 in the x direction; (c) The equilibrium path of node 2 in the z direction; (d) The equilibrium path of node 4 in the x direction; (e) The equilibrium path of node 4 in the z direction; (f) The equilibrium path of node 5 in the x direction; (g) The equilibrium path of node 5 in the z direction.



(d)



(e)



(f)

Figure 9. (Continued)

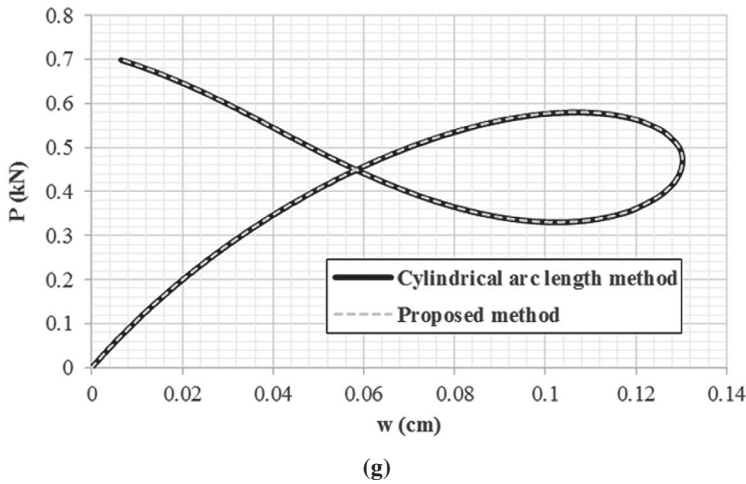


Figure 9. (Continued)

with various initial deficiencies of the members, was analysed by the exact and tangential stiffness matrix of the beam-column member with initial curvature (Chan & Gu, 2000).

The obtained diagrams for nodes 1 and 2 in this space frame are shown in Figure 5. Accordingly, the load limit points are observed in the structural equilibrium paths of both nodes. Furthermore, the behavioural curves of node 2 have a displacement limit point in both directions. Once again, it is clear that the suggested method can trace these complex paths accurately.

The obtained results are inserted in Table 2. Similarly, these outcomes indicate the interpretation of the previous subsection.

3.3. Star-shaped frame with low rigidity under symmetric loading pattern

This space frame is demonstrated in Figure 6. A concentrated load, P , is applied to node 1 and nodes 2–7 are subjected to load $\frac{P}{2}$. The elasticity and shear modulus of the members are $E = 303 \text{ kN/cm}^2$ and $G = 109.6 \text{ kN/cm}^2$, respectively. The cross-sectional area, the moment of inertia about the y and z axes are $A = 3.17 \text{ cm}^2$, $I_y = .295 \text{ cm}^4$, and $I_z = 2.377 \text{ cm}^4$, correspondingly. Moreover, the member torsional moment of inertia is equal to $J = .918 \text{ cm}^4$. It should be reminded that this symmetric loading pattern of the three-dimensional structure was examined by Meek and Tan (Meek & Tan, 1984).

In a similar manner to the previous samples, the amazing equilibrium curves for nodes 1 and 2 emerge. Based on Figure 7(a), the equilibrium path of the middle node includes two load limit points, which can be successfully passed by the suggested approach. According to Figure 7(b), as for the static curve of node 2 in the x direction, not only authors' strategy passes the snap-through region, but also is capable of catching the snap-back one. Moreover, the equilibrium path of

Table 3. The number of the increments and iterations of the star-shaped frame with low rigidity under symmetric loading pattern.

Technique	Number of increments	Number of iterations
Proposed method	506	3592
Cylindrical arc length method	708	2690

node 2 in the z direction has two displacement limit points. Based on the obtained responses, the new tactic can trace these complex curves completely.

It should be mentioned that the new method requires 506 increments and 3592 iterations for performing the nonlinear analysis of this star-shaped frame. According to Table 3, the cylindrical arc length scheme needs more increments and fewer iterations in comparison to authors' tactic for tracing the equilibrium curves of this space structure.

3.4. Star-shaped frame with low rigidity under asymmetric loading pattern

Figure 8 illustrates this 3D frame subjected to an asymmetric loading pattern. The concentrated load, $\frac{P}{2}$, is applied to nodes 2, 3 and 7, and also load P is exerted to the central node. The physical and mechanical properties of the members are analogous to those of the previous example. It should be noted that, this space structure was analysed by the other researchers, as well (Meek & Tan, 1984).

Fourteen non-linear analyses are performed on this frame. The equilibrium paths for nodes 1, 2, 4 and 5 are illustrated in Figure 9. By comparing Figures 7 and 9, it can be concluded that the structural equilibrium paths of the frame under asymmetric loading pattern include sharper curvatures. It should be remarked that nodes 4 and 5 are not subjected to any loads, and their equilibrium paths are complicated. It is worthwhile to highlight that the suggested method can successfully trace all mentioned paths. Note that; all obtained results are compatible with those of the other researchers (Meek & Tan, 1984).

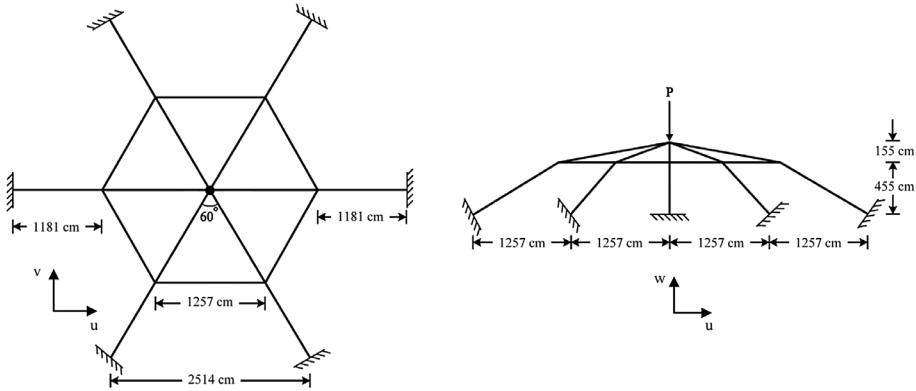
As it was mentioned throughout the text; the presented approach does not have a predictor step, so it works automatically. The number of the required increments and iterations are listed in Table 4. Consequently, authors' technique is slower than the cylindrical arc length tactic for this benchmark sample.

3.5. Dome frame

This space frame has 18 members and 43 nodes. As demonstrated in Figure 10, the central node is subjected to a concentrated load, P , and the ends of the peripheral members are fixed. The elasticity and shear modulus of all members are $E = 2069 \text{ kN/cm}^2$ and $G = 883 \text{ kN/cm}^2$, respectively. The cross-sectional area and flexural moments of inertia are $A = 9272 \text{ cm}^2$, $I_y = 1.15 \times 10^7 \text{ cm}^4$, and $I_z = 4.463 \times 10^6 \text{ cm}^4$, correspondingly. Moreover, the member torsional moment of inertia is equal to $J = 1.93 \times 10^7 \text{ cm}^4$. In 1982, the frame dome with large deformations

Table 4. The number of the increments and iterations of the star-shaped frame with low rigidity under asymmetric loading pattern.

Technique	Number of increments	Number of iterations
Proposed method	529	3756
Cylindrical arc length method	742	2819

**Figure 10.** The plan and view of the dome frame.

was analysed by the finite element method (Argyris, Boni, Hindenlang, & Kleiber, 1982). Papadrakakis and Ghionis solved this benchmark sample by the conjugate gradient algorithms (Papadrakakis & Ghionis, 1986). Later, the technique based on Euler's formulation was used for analysing this structure (Kassimali & Abbasnia, 1991). For geometrically non-linear behaviour, Park and Lee solved this 3D frame with shear beam element (Park & Lee, 1996). Recently, the frame dome was considered in the analysis of the 3D Timoshenko frames having the geometrical and material nonlinear behaviours by Rezaiee-Pajand and Gharaei-Moghaddam (Rezaiee-Pajand & Gharaei-Moghaddam, 2015). In the current paper, each frame member is divided into three elements to perform nonlinear analysis. Therefore, this three-dimensional frame is analysed by 54 elements.

Herein, the equilibrium path of the highest node in the loaded direction is represented. According to Figure 11, the obtained results of the new tactic are well-matched with those achieved by the cylindrical arc length algorithm and other researchers' techniques. If this 3D dome frame has the members with low rigidity, the snap-through region appears on the related equilibrium path, like the analysed star-shaped frame with high rigidity in comparison to low rigid one.

In this part, the suggested approach is compared to the cylindrical arc length technique. The number of the required increments and iterations of authors' strategy are 232 and 1879, respectively. However, the cylindrical arc length scheme needs 302 increments and 1268 iterations to trace the equilibrium path. It is worth emphasising that the achieved results are completely adaptable with those of the previous studies (Kassimali & Abbasnia, 1991; Papadrakakis & Ghionis, 1986; Park & Lee, 1996; Rezaiee-Pajand & Gharaei-Moghaddam, 2015).

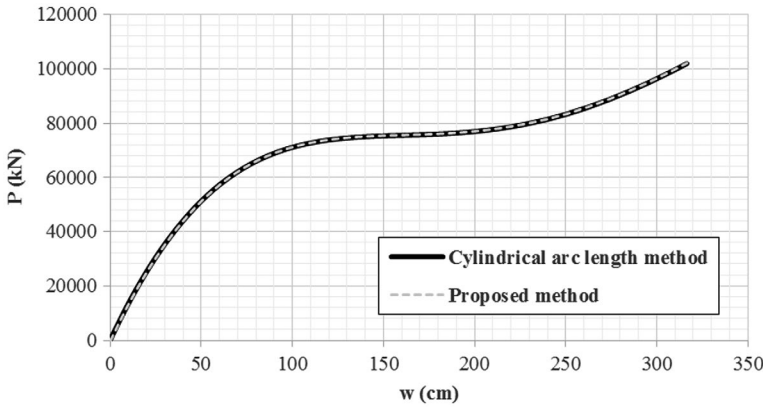


Figure 11. The equilibrium path corresponding to the dome frame's node under a concentrated load.

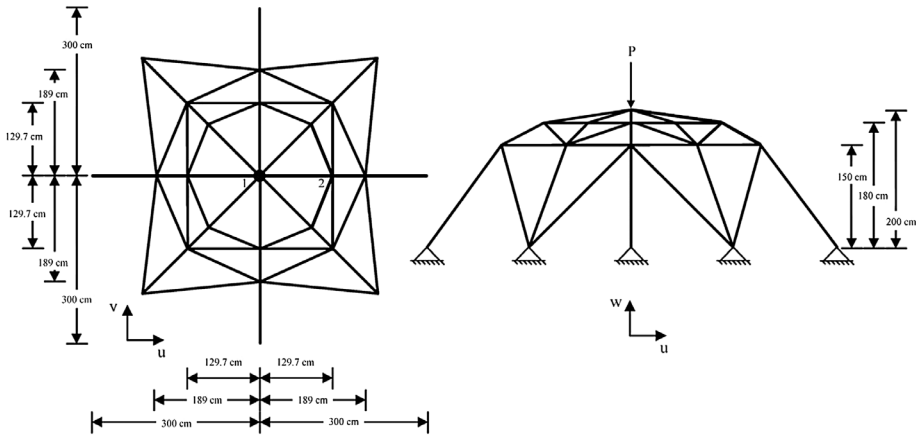


Figure 12. The plan and view of the 64-member space frame.

3.6. 64-member space frame

This frame has eight simple supports, and a concentrated load P is applied to the peak node. Figure 12 shows the 64-member space frame. Members' cross-sectional areas are considered to be $A = 100 \text{ cm}^2$. The bending moments of inertia of all members are assumed to be $I_y = I_z = 5000 \text{ cm}^4$, and the torsional moments of inertia of them are supposed to be $J = 5000 \text{ cm}^4$. Besides, the elasticity and shear modulus are $E = 20.6 \text{ kN/cm}^2$ and $G = 7.92 \text{ kN/cm}^2$, respectively.

For verification, the suggested method is utilised in a companion with the cylindrical arc length scheme. The nonlinear analysis of this structure is carried out four times. Firstly, the structural equilibrium curve of node 1 in the z direction is determined. Based on Figure 13(a), the novel method can automatically perform the geometric nonlinear analysis of this space structure. Whereas, the cylindrical

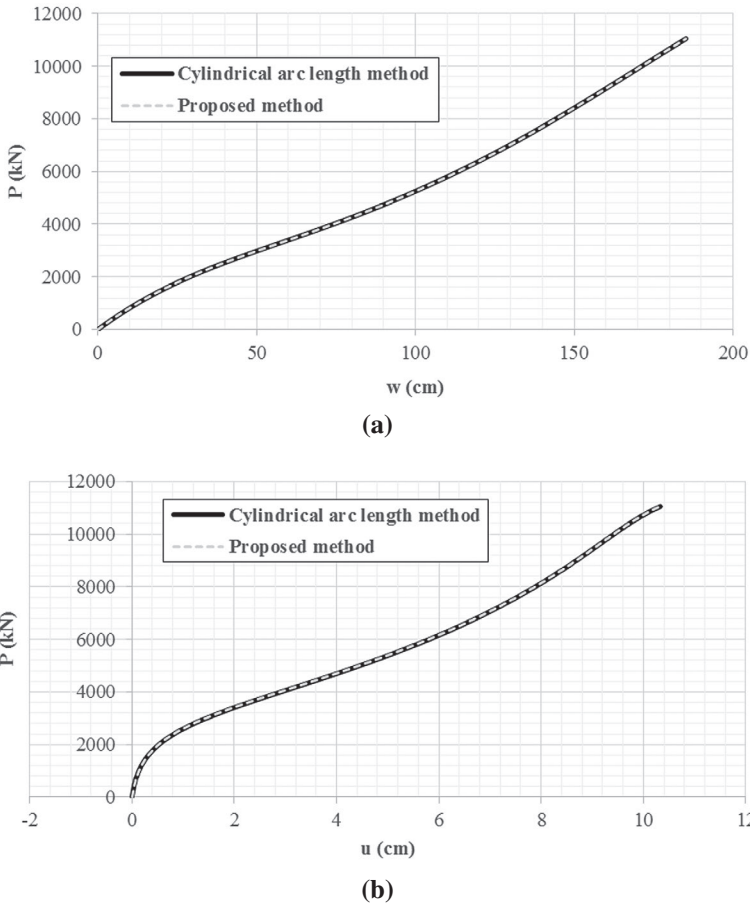


Figure 13. The structural static curves of the 64-member frame. (a) The equilibrium path of node 1 in the z direction; (b) The equilibrium path of node 2 in the x direction.

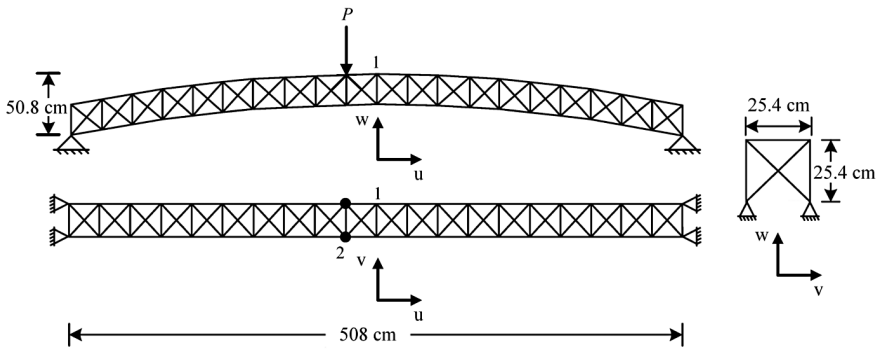


Figure 14. The longitudinal view, transversal view, and plan of the arch frame.

arc length tactic requires the predictor step for the analysis. Secondly, the frame response for node 2 in the x direction is located. In Figure 13(b), the ability of authors' scheme in tracing the equilibrium path of this frame is displayed.

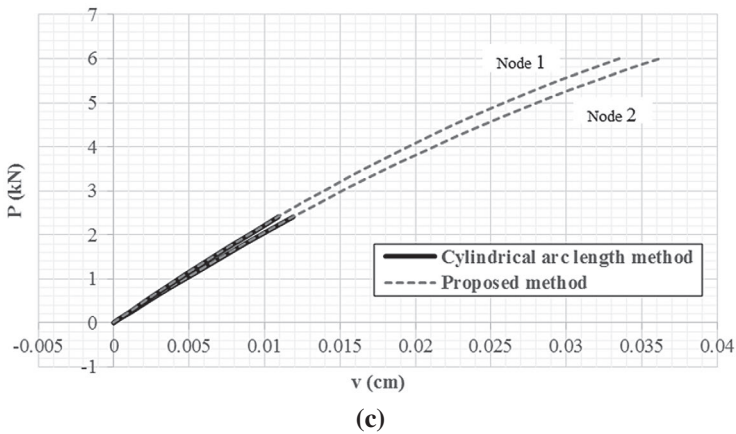
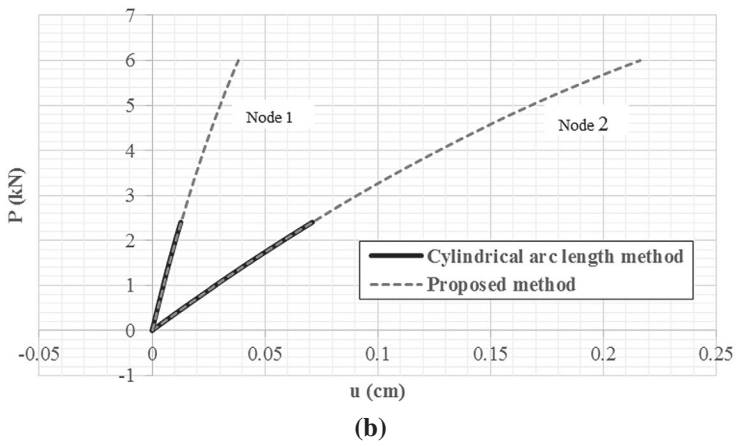
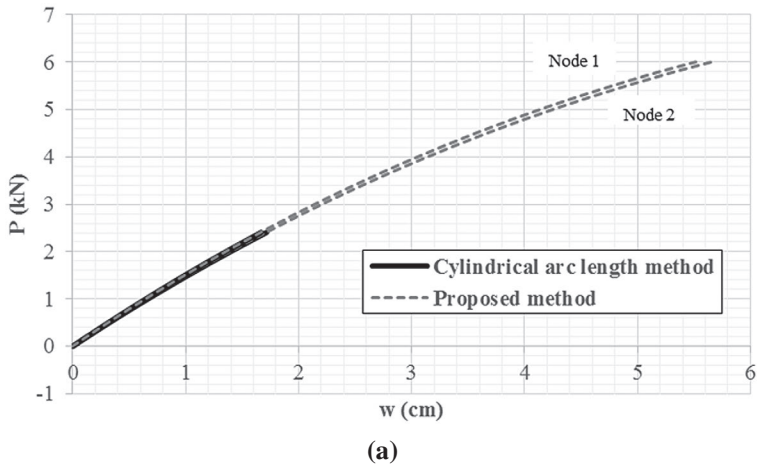


Figure 15. The force-deformation diagrams of the arch frame. (a) The structural static curves in the z direction; (b) The structural static curves in the x direction; (c) The structural static curves in the y direction.

Lastly, the required numbers of the increments and iterations for the nonlinear analysis are presented. The novel strategy traces the equilibrium paths of Figure 13 using 495 increments and 3712 iterations. Moreover, the cylindrical arc length scheme needs 743 increments and 3789 iterations so as to trace the mentioned equilibrium paths. Evidently, the new algorithm is a bit faster than the cylindrical arc length method for this space frame.

3.7. Arch frame

The arch structure shown in Figure 14, has 267 members and 84 nodes. Two concentrated loads with an asymmetric pattern are applied to this frame. The cross-sectional area, the member flexural and torsional moments of inertia are presumed to be $A = 20.45 \text{ cm}^2$, $I_y = I_z = 34.84 \text{ cm}^4$, and $J = 58.73 \text{ cm}^4$, correspondingly. In addition, the elasticity and shear modulus of all members are considered to be $E = 208.9 \text{ kN/cm}^2$ and $G = 75.57 \text{ kN/cm}^2$, respectively.

Firstly, the equilibrium paths of nodes 1 and 2, in the z direction, are found. In the subsequent examinations, the designed frame is analysed for these nodes in the x and y directions.

According to Figure 15(a), it is clear that the suggested tactic can completely trace the equilibrium paths of both nodes in the z direction. In contrast, the cylindrical arc length procedure can only trace the beginning parts of these paths. As it can be seen in Figure 15(b), authors' scheme successfully finds the load-displacement diagrams of the mentioned nodes in the x direction. However, the cylindrical arc length strategy cannot trace the related paths, thoroughly. As for the y direction, the similar results can be observed, based on Figure 15(c). Regarding to these issues, the novel method can represent the total static curves of the mentioned frame, which has the most number of degrees of freedom in the presented numerical examples. Whereas, utilising the cylindrical arc length technique is not appropriate for this space structure. It can be concluded that authors' technique is more efficient than the cylindrical arc length strategy in analysing this 3D arch structure.

4. Conclusion

In order to perform the incremental-iterative processes, the load factor increment is obtained by applying the constraint equation. To develop this relation, the path of the iterative analyses was assumed to be a parabolic curve. By employing the mathematical principles and applying two different procedures, a novel constraint equation was derived. Reaching the same constraint equality for the suggested approaches by these two diverse ways, somehow verified the accuracy of authors' assumptions and formulations. In contrast to the common ways, the presented scheme does not require the predictor step. Besides, no try and errors are needed by the analyst to adjust properly the predictor value for solving problems. Hence,

authors' technique can analyse the structures automatically. It should be reminded that the previous similar strategies required the predictor step. Consequently, an initial approximation could enter to their formulations. The second superiority of the new formulation is that the proposed constraint equation is single-valued. As a result, there is no need to select an appropriate load factor increment among the roots. To affirm the capability of the proposed method, various numerical tests were performed. These evaluations and the related outcomes proved the high ability of the new approach in passing all types of the limit points. Moreover, this novel strategy can trace the equilibrium paths perfectly. After solving the benchmark problems, it was found that the obtained results were compatible entirely with those accomplished by the other researchers.

Notations

R	residual load vector
u	displacement vector
λ	load factor
P	external force vector
F	internal force vector
m	number of degrees of freedom
n	increment number
i	iteration number
K	tangential stiffness matrix
Δ	increment in predictor step
δ	increment in corrector step
$\delta u''$	displacement increment due to residual load
$\delta u'$	displacement increment due to external force
a, b, c	coefficients of parabolic equation
Λ	load factor of transferred coordinate system
U	displacement vector of transferred coordinate system
L	arc length of iterative path
E	elasticity modulus
G	shear modulus
A	cross-sectional area
I	bending moment
J	torsional moment
x, y, z	main directions of Cartesian coordinate axes
u, v, w	nodal displacements in x, y and z directions

Disclosure statement

No potential conflict of interest was reported by the authors.

ORCID

Mohammad Rezaiee-Pajand  <http://orcid.org/0000-0002-8808-0011>

References

- Allgower, E. L., & Georg, K. (1979). Homotopy methods for approximating several solutions to nonlinear systems of equations. *Numerical Solution of Highly Nonlinear Problems*, W. Forster, North-Holland, 72, 253–270.
- Argyris, J. H., Boni, B., Hindenlang, U., & Kleiber, M. (1982). Finite element analysis of two- and three-dimensional elasto-plastic frames-the natural approach. *Computer Methods in Applied Mechanics and Engineering*, 35(2), 221–248.
- Batoz, J. L., & Dhatt, G. (1979). Incremental displacement algorithms for nonlinear problems. *International Journal for Numerical Methods in Engineering*, 14(8), 1262–1267.
- Bergan, P. G. (1980). Solution algorithms for nonlinear structural problems. *Computers and Structures*, 12(4), 497–509.
- Cardoso, E. L., & Fonseca, J. S. O. (2007). The GDC method as an orthogonal arc-length method. *Communications in Numerical Methods in Engineering*, 23(4), 263–271.
- Chajes, A., & Churchill, J. E. (1987). Nonlinear frame analysis by finite element methods. *Journal of Structural Engineering, ASCE*, 113(6), 1221–1235.
- Chan, S. L. (1988). Geometric and material non-linear analysis of beam-columns and frames using the minimum residual displacement method. *International Journal for Numerical Methods in Engineering*, 26(12), 2657–2669.
- Chan, S. L., & Gu, J. X. (2000). Exact tangent stiffness for imperfect beam-column members. *Journal of Structural Engineering, ASCE*, 126(9), 1094–1102.
- Chang, J. T. (2004). Derivation of the higher-order stiffness matrix of a space frame element. *Finite Elements in Analysis and Design*, 41(1), 15–30.
- Connor, J. J., Logcher, R. D., & Chan, S. C. (1968). Nonlinear analysis of elastic framed structures. *Journal of the Structural Division, ASCE*, 94(6), 1525–1547.
- Crisfield, M. A. (1979). A faster modified Newton-Raphson iteration. *Computer Methods in Applied Mechanics and Engineering*, 20(3), 267–278.
- Crisfield, M. A. (1981). A fast incremental/iterative solution procedure that handles “snap-through”. *Computers and Structures*, 13(1), 55–62.
- Fried, I. (1984). Orthogonal trajectory accession to the nonlinear equilibrium curve. *Computer Methods in Applied Mechanics and Engineering*, 47(3), 283–297.
- Hsiao, K. M., Horng, H. J., & Chen, Y. R. (1987). A corotational procedure that handles large rotations of spatial beam structures. *Computers and Structures*, 27(6), 769–781.
- Kassimali, A., & Abbasnia, R. (1991). Large deformation analysis of elastic space frames. *Journal of Structural Engineering, ASCE*, 117(7), 2069–2087.
- Kim, J. H., & Kim, Y. H. (2001). A predictor-corrector method for structural nonlinear analysis. *Computer Methods in Applied Mechanics and Engineering*, 191(8–10), 959–974.
- Krenk, S., & Hededal, O. (1995). A dual orthogonality procedure for non-linear finite element equations. *Computer Methods in Applied Mechanics and Engineering*, 123(1–4), 95–107.
- Krishnamoorthy, C. S., Ramesh, G., & Dinesh, K. U. (1996). Post-buckling analysis of structures by three-parameter constrained solution techniques. *Finite Elements in Analysis and Design*, 22(2), 109–142.

- Ligaro, S. S., & Valvo, P. S. (2006). Large displacement analysis of elastic pyramidal trusses. *International Journal of Solids and Structures*, 43(16), 4867–4887.
- Meek, J. L., & Loganathan, S. (1989). Large displacement analysis of space-frame structures. *Computer Methods in Applied Mechanics and Engineering*, 72(1), 57–75.
- Meek, J. L., & Tan, H. S. (1984). Geometrically nonlinear analysis of space frames by an incremental iterative technique. *Computer Methods in Applied Mechanics and Engineering*, 47(3), 261–282.
- Meek, J. L., & Xue, Q. (1998). A study on the instability problem for 3D frames. *Computer Methods in Applied Mechanics and Engineering*, 158(3-4), 235–254.
- Oran, C. (1973a). Tangent stiffness in plane frames. *Journal of the Structural Division, ASCE*, 99(6), 973–985.
- Oran, C. (1973b). Tangent stiffness in space frames. *Journal of the Structural Division, ASCE*, 99(6), 987–1001.
- Papadrakakis, M. (1983). Inelastic post-buckling analysis of trusses. *Journal of Structural Engineering, ASCE*, 109(9), 2129–2147.
- Papadrakakis, M., & Ghionis, P. (1986). Conjugate gradient algorithms in nonlinear structural analysis problems. *Computer Methods in Applied Mechanics and Engineering*, 59(1), 11–27.
- Park, M. S., & Lee, B. C. (1996). Geometrically non-linear and elastoplastic three-dimensional shear flexible beam element of Von-Mises-type hardening material. *International Journal for Numerical Methods in Engineering*, 39(3), 383–408.
- Powell, G., & Simons, J. (1981). Improved iteration strategy for nonlinear structures. *International Journal for Numerical Methods in Engineering*, 17(10), 1455–1467.
- Ramm, E. (1981). Strategies for tracing the nonlinear response near limit points. In W. Wunderlich, E. Stein, & K. J. Bathe (Eds.), *Nonlinear finite element analysis in structural mechanics* (pp. 63–89). Berlin, Heidelberg: Springer.
- Rezaiee-Pajand, M., & Afsharimoghadam, H. (2017). Optimization formulation for nonlinear structural analysis. *International Journal of Optimization in Civil Engineering*, 7(1), 109–127.
- Rezaiee-Pajand, M., & Alamatian, J. (2008). Nonlinear dynamic analysis by dynamic relaxation method. *Structural Engineering and Mechanics*, 28(5), 549–570.
- Rezaiee-Pajand, M., & Alamatian, J. (2010). The dynamic relaxation method using new formulation for fictitious mass and damping. *Structural Engineering and Mechanics*, 34(1), 109–133.
- Rezaiee-Pajand, M., & Alamatian, J. (2011). Automatic DR structural analysis of snap-through and snap-back using optimized load increments. *Journal of Structural Engineering, ASCE*, 137(1), 109–116.
- Rezaiee-Pajand, M., & Boroshaki, F. (1999). A variable arc-length method. *Asian Journal of Structural Engineering*, 3, 21–44.
- Rezaiee-Pajand, M., & Estiri, H. (2016a). Mixing dynamic relaxation method with load factor and displacement increments. *Computers and Structures*, 168, 78–91.
- Rezaiee-Pajand, M., & Estiri, H. (2016b). Computing the structural buckling limit load by using dynamic relaxation method. *International Journal of Non-Linear Mechanics*, 81, 245–260.
- Rezaiee-Pajand, M., & Estiri, H. (2016c). A comparison of large deflection analysis of bending plates by dynamic relaxation. *Periodica Polytechnica Civil Engineering*, 60(4), 619–645.
- Rezaiee-Pajand, M., & Estiri, H. (2016d). Finding equilibrium paths by minimizing external work in dynamic relaxation method. *Applied Mathematical Modelling*, 40, 10300–10322.
- Rezaiee-Pajand, M., & Gharaei-Moghaddam, N. (2015). Analysis of 3D Timoshenko frames having geometrical and material nonlinearities. *International Journal of Mechanical Sciences*, 94, 140–155.
- Rezaiee-Pajand, M., & Rezaee, H. (2014). Fictitious time step for the kinetic dynamic relaxation method. *Mechanics of Advanced Materials and Structures*, 21(8), 631–644.

- Rezaiee-Pajand, M., & Sarafrazi, S. R. (2010). Nonlinear structural analysis using dynamic relaxation method with improved convergence rate. *International Journal of Computational Methods*, 7(4), 627–654.
- Rezaiee-Pajand, M., & Sarafrazi, S. R. (2011). Nonlinear dynamic structural analysis using dynamic relaxation with zero damping. *Computers and Structures*, 89(13–14), 1274–1285.
- Rezaiee-Pajand, M., & Taghavian-Hakkak, M. (2006). Nonlinear analysis of truss structures using dynamic relaxation (research note). *International Journal of Engineering-Transactions B: Applications*, 19(1), 11–22.
- Rezaiee-Pajand, M., & Tatar, M. (2006). Some orthogonal methods for geometric nonlinear analysis. *International Journal of Engineering Science, Iran University of Science and Technology*, 17(2), 35–41 (In Persian).
- Rezaiee-Pajand, M., & Tatar, M. (2009). The solution of nonlinear finite element equations with minimizing of residual factors. *Technical and Engineering Journal of Modares*, 35, 17–28 (In Persian).
- Rezaiee-Pajand, M., Tatar, M., & Moghaddasie, B. (2009). Some geometrical bases for incremental-iterative methods (research note). *International Journal of Engineering-Transactions B: Applications*, 22(3), 245–256.
- Rezaiee-Pajand, M., Kadkhodayan, M., Alamatian, J., & Zhang, L. C. (2011). A new method of fictitious viscous damping determination for the dynamic relaxation method. *Computers and Structures*, 89(9–10), 783–794.
- Rezaiee-Pajand, M., Kadkhodayan, M., & Alamatian, J. (2012). Timestep selection for dynamic relaxation method. *Mechanics Based Design of Structures and Machines*, 40(1), 42–72.
- Rezaiee-Pajand, M., Sarafrazi, S. R., & Rezaiee, H. (2012). Efficiency of dynamic relaxation methods in nonlinear analysis of truss and frame structures. *Computers and Structures*, 112–113, 295–310.
- Rezaiee-Pajand, M., Ghalishooyan, M., & Salehi-Ahmadabad, M. (2013). Comprehensive evaluation of structural geometrical nonlinear solution techniques Part I: Formulation and characteristics of the methods. *Structural Engineering and Mechanics*, 48(6), 849–878.
- Riks, E. (1972). The application of Newton's method to the problem of elastic stability. *Journal of Applied Mechanics, ASCE*, 39(4), 1060–1065.
- Riks, E. (1979). An incremental approach to the solution of snapping and buckling problems. *International Journal of Solids and Structures*, 15(7), 529–551.
- Saafan, S. A. (1965). Nonlinear behavior of structural plane frames. *Journal of the Structural Division, ASCE*, 89(4), 557–579.
- Saffari, H., Fadaee, M. J., & Tabatabaei, R. (2008). Nonlinear analysis of space trusses using modified normal flow algorithm. *Journal of Structural Engineering, ASCE*, 134(6), 998–1005.
- Simons, J., Bergan, P. G., & Nygard, M. K. (1984). Hyperplane displacement control methods in nonlinear analysis. *Proceedings of the International Conference on Innovative Methods for Nonlinear Problems*, (pp. 345–364). Pineridge Press International.
- Singh, H., & Singh, G. M. (1992). Non-linear analysis of frames. *Computers and Structures*, 44(6), 1377–1379.
- Spillers, W. R. (1990). Geometric stiffness matrix for space frames. *Computers and Structures*, 36(1), 29–37.
- Tezcan, S. S., & Mahapatra, B. C. (1969). Tangent stiffness matrix of space frame members. *Journal of the Structural Division, ASCE*, 95(6), 1257–1270.
- Toklu, Y. C. (2004). Nonlinear analysis of trusses through energy minimization. *Computers and Structures*, 82(20–21), 1581–1589.
- Torkamani, M. A. M., Sonmez, M., & Cao, J. (1997). Second-order elastic plane-frame analysis using finite-element method. *Journal of Structural Engineering, ASCE*, 123(9), 1225–1235.

- Wempner, G. A. (1971). Discrete approximations related to nonlinear theories of solids. *International Journal of Solids and Structures*, 7(11), 1581–1599.
- Wen, R. K., & Rahimzadeh, J. (1983). Nonlinear elastic frame analysis by finite element. *Journal of Structural Engineering, ASCE*, 109(8), 1952–1971.
- Yang, T. Y. (1973). Matrix displacement solution to elastica problems of beams and frames. *International Journal of Solids and Structures*, 9(7), 829–842.
- Yang, Y. B., & McGuire W. (1985). A work control method for geometrically nonlinear analysis. Proceedings of International Conference on Numerical Methods in Engineering: Theory and Applications (pp. 913–921). Swansea: University College of Swansea.
- Yang, Y. B., & McGuire, W. (1986). Stiffness matrix for geometric nonlinear analysis. *Journal of Structural Engineering, ASCE*, 112(4), 853–877.
- Yang, Y. B., & Shieh, M. S. (1990). Solution method for nonlinear problems with multiple critical points. *AIAA Journal*, 28(12), 2110–2116.
- Yang, Y. B., Lin, S. P., & Wang, C. M. (2007). Rigid element approach for deriving the geometric stiffness of curved beams for use in buckling analysis. *Journal of Structural Engineering, ASCE*, 133(12), 1762–1771.
- Zienkiewicz, O. C. (1971). Incremental displacement in non-linear analysis. *International Journal for Numerical Methods in Engineering*, 3(4), 587–588.